

Scanned-Spot-Array Imaging Systems

Kenneth C. Johnson

KJ Innovation, 2502 Robertson Rd, Santa Clara, CA 95051, USA
kjinnovation@earthlink.net kjinnovation.com

Abstract: Scanned-spot-array imaging systems have utility for maskless lithography and parallel confocal microscopy. Such systems can be configured to neutralize geometric optical aberrations of a projection lens and achieve perfect point-imaging performance, free of field curvature and distortion, over a wide image field at high numerical aperture. This is possible because the beam-forming micro-optics for each individual spot need only be optimized for a single image point. Furthermore, the micro-optics can employ phase-Fresnel surfaces to achieve narrow-band achromatization (e.g. to avoid the need for laser line narrowing in microlithography), and can employ form-birefringent surfaces to optimally control the image field's polarization state.

©2011 Kenneth C. Johnson (Version Nov. 10, 2011)

References and links

1. T. Matsuyama, Y. Ohmura and D. M. Williamson, "The Lithographic Lens: its history and evolution," Proc. SPIE **6154**, 615403 (2006).
 2. K. Johnson, "Microlens Scanner for Microlithography and Wide-Field Confocal Microscopy," U.S. Patent 6,133,986 (2000).
 3. K. Johnson, "High-Throughput, Maskless Lithography System," U.S. Patent 6,177,980 (2001)
 4. LumArray, Inc., <http://lumarray.com/>.
 5. M. Fritze, B. Tyrrell, D. Astolfi, D. Yost, P. Davis, B. Wheeler, R. Mallen, J. Jarmolowicz, and S. Cann, "Gratings of regular arrays and trim exposures for ultralarge scale integrated circuit phase-shift lithography," J. Vac. Sci. Technol. B **19**(6)?, 2366-2370 (2001).
 6. K. Johnson, "Spot-Array Imaging System for Maskless Lithography and Parallel Confocal Microscopy," U.S. Provisional Patent Application No. 61/549,158 (2011). (Available from author.)
 7. K. Miyamoto, "The Phase Fresnel Lens," J. Opt. Soc. Am. **51**(1), 17-20 (1961).
 8. K. Johnson, "Dispersion-compensated fresnel lens," U.S. Patent 5,161,057 (1992).
 9. D. Faklis and G. M. Morris, "Polychromatic diffractive lens," U.S. Patent 5,589,982 (1996).
 10. M. Born and E. Wolf, *Principles of Optics*, 7th Ed. (Cambridge University Press, 1999), Chap. 3.
 11. I. H. Malitson, "Interspecimen Comparison of the Refractive Index of Fused Silica," J. Opt. Soc. Am. **55**(10), 1205-1209 (1965).
 12. Kenneth Johnson, "Cornu Spline," posted on MATLAB Central File Exchange (2011), <http://www.mathworks.com/matlabcentral/fileexchange/33594-cornu-spline>.
 13. R. Petit, M. Cadilhac, D. Maystre, P. Vincent, M. Nevière, R. C. McPhedran, G. H. Derrick, and L. C. Botten, *Electromagnetic Theory of Gratings*, R. Petit, ed. (Springer-Verlag, Berlin, 1980).
 14. J. H. Burnett, E. C. Benck, S. G. Kaplan, G. Y. Sirat, and C. Mack, "Birefringence issues with uniaxial crystals as last lens elements for high-index immersion lithography," Proc. SPIE **7274**, 727421 (2009).
 15. I. Richter, P. Sun, F. Xu, and Y. Fainman, "Design considerations of form birefringent microstructures," Appl. Opt. **34**(14), 2421-2429 (1995).
 16. Z. Bomzon, G. Biener, V. Kleiner, and E. Hasman, "Radially and azimuthally polarized beams generated by space-variant dielectric subwavelength gratings," Optics Letters **27**(5), 285-287 (2002).
 17. GD-Calc® (Grating Diffraction Calculator), <http://software.kjinnovation.com/GD-Calc.html>.
-

1. Background

Optical image projection systems such as those used for microlithography and semiconductor inspection entail a balance of tradeoffs to achieve high-numerical-aperture imaging with minimal field curvature, distortion, and aberration over a wide image field. These tradeoffs lead to complex and expensive optical systems. For example, lithographic lenses can stand over one meter tall, weigh one tonne, and comprise about 50 sequential optical surfaces including aspherics [1]. Moreover, even with substantially perfect optical imaging the need for optical proximity correction in photomask design complexifies mask-projection lithography processes, and inspection microscopy is similarly affected by coherent proximity effects.

These difficulties can be circumvented, in principle, by employing a scanned-spot-array imaging system such as that illustrated schematically in Fig. 1(a) (in a lithography embodiment) and in Fig. 1(b) (in a parallel-confocal-microscopy embodiment) [2, 3]. In Fig. 1(a), illumination is directed onto a spatial light modulator (SLM) by means of a beam splitter, and the SLM is imaged by a projection lens onto a microlens array, with each SLM pixel being imaged onto a particular corresponding microlens. (The number of microlenses could be of order one million.) The microlenses condense the image radiation onto diffraction-limited focused spots on a printing surface, which is raster-scanned across the spot array, as illustrated in Fig. 2, to expose a digitally synthesized, full-field lithographic image. The microscopy system (Fig. 1(b)) employs similar imaging optics, but in this case the illumination is directed through the projection lens and microlens array onto a scanned inspection surface and the radiation reflected from the surface is projected back through the optics onto a detector array.

The separation of the image radiation into discrete focal spots eliminates coherent optical proximity effects and the need for optical proximity correction in the context of lithography. In the context of microscopy the spot partitioning results in the characteristic high image resolution and depth discrimination of confocal microscopy systems.

The Fig. 1(a) system is currently being commercialized by LumArray Inc. with its ZP-150 product, which uses a 1000-pixel SLM and a Fresnel zone-plate microlens array [4]. The system's writing speed is limited by the SLM, but for applications that only require the printing of periodic patterns this constraint could be overcome by eliminating the SLM and simply providing uniform, source-modulated illumination to the entire microlens array. This technique would be similar to the GRATE approach ("Gratings of Regular Arrays and Trim Exposures" [5]), except that the periodicity constraint would be much less limiting. (With source modulation the maximum pattern period would be, e.g., 100 micron for a zone-plate system having a 100-micron microlens center spacing, in contrast to the sub-micron period with GRATE.)

A system such as that of Fig. 1(a) or Fig. 1(b) can use a simple, low-resolution projection lens, but the tradeoff to this advantage is that it requires very small, high-numerical-aperture microlenses operating in close proximity to the printing or inspection surface. The zone-plate lenses used in LumArray's system can achieve diffraction-limited, high-NA point focusing performance, but less than half of the diffracted light goes into the first diffracted order. Moreover, such systems have not been adapted for immersion imaging (either immersion microscopy or immersion lithography).

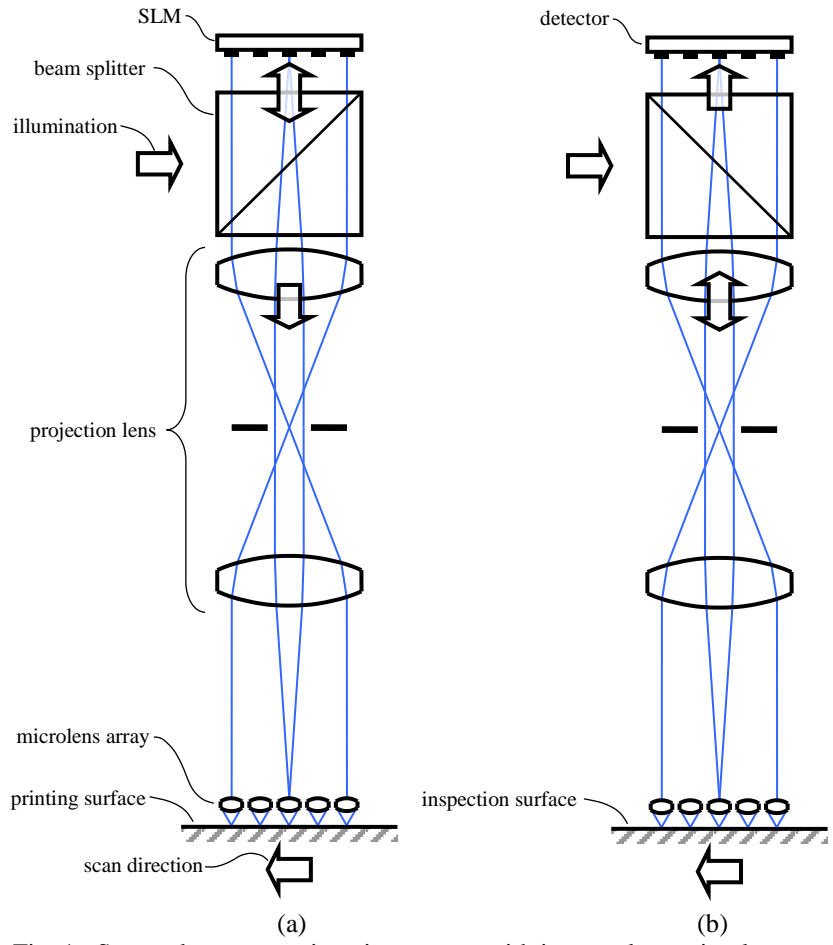


Fig. 1. Scanned-spot-array imaging system with image-plane microlens array, configured for (a) maskless lithography and (b) parallel confocal microscopy.

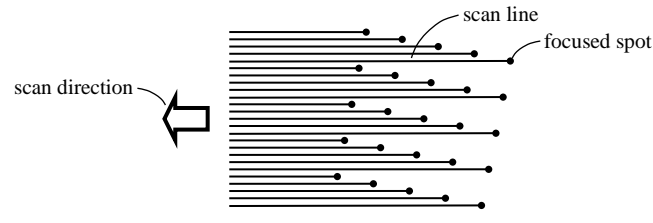


Fig. 2. Raster scan

The micro-optics design and fabrication can be greatly simplified by generating the spots in the object space of projection lens, which images the spot array onto the image plane at reduced magnification. Figure 3 shows a schematic illustration of such a system. (The figure is primarily illustrative of a lithography system, but the same optical configuration could be used for confocal microscopy.) If a typical 5X-reduction lithographic projection lens is employed then the individual microlens aperture dimensions would be increased by a factor of 5, and their numerical apertures would be reduced by a factor of 5, relative to the Fig. 1(a) system (to achieve the same image-plane spot density). Moreover, the microlens foci can be spatially filtered by means of a focal-plane aperture array. The microlenses could be formed,

for example, as a grey-scale-etched pattern of refractive lens elements formed by an interference lithography technique on the top side of a photomask plate; and the aperture array could be formed on the plate's bottom surface using a self-aligned lithographic process in which exposure radiation is focused through the microlenses.

The Fig. 3 system could use a state-of-the art projection lens. Figure 4 depicts one such lens, which stands about one meter tall [1]. It might appear that the advantage of generating the spot array in the projection lens's object space is nullified by the increased complexity of the lens, but that is actually not the case because the spot-generation micro-optics can be designed to supplant much of the projection lens functionality [6]. Specifically, the micro-optics can directly control field flatness, distortion, geometric aberration, chromatic aberration, polarization, and beam intensity.

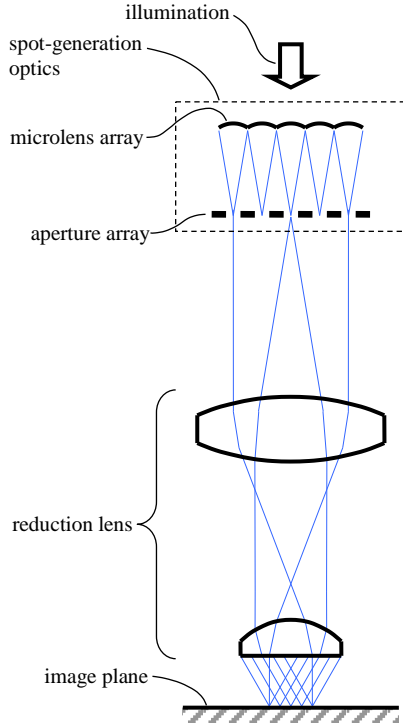


Fig. 3. Scanned-spot-array imaging system with spots generated in object space.

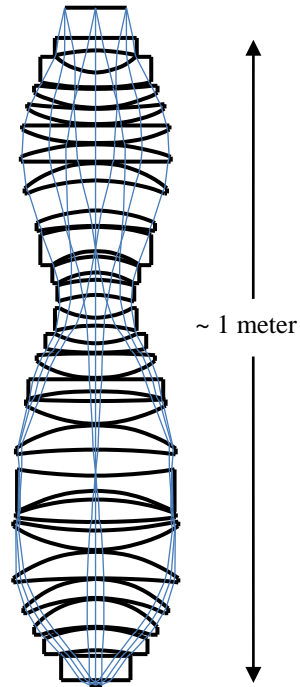


Fig. 4. Conventional microlithographic reduction lens (0.85 NA, 193 nm)

2. Elimination of field curvature, distortion, and geometric aberration

The double-bulge shape of the projection lens illustrated in Fig. 4 is a consequence of the need to achieve flat-field imaging performance (i.e., the strong negative elements are needed to minimize the lens's Petzval sum). However, no such design constraint need be applied in the context of the Fig. 3 system because the object spots need not be confined to a plane. Figure 5 schematically illustrates spot-generation optics that focus the object spots onto a curved object surface. The surface shape can be configured to compensate for the projection lens's field curvature so that the conjugate image points are on a perfectly flat image surface.

The projection lens similarly need not achieve a stringent distortion specification because the object spot distribution can be configured to compensate for any lens distortion. A non-periodic spot layout pattern in the object space (Fig. 5) can be defined to achieve a perfectly periodic image-plane spot array.

Furthermore, the projection lens need not achieve accurate point-imaging performance because the microlenses can be configured to achieve a perfect geometric point images at the image plane even in the presence of large projection lens aberrations. The microlens foci in the object space would be slightly aberrated (Fig. 5) in a manner that counterbalances and neutralizes the projection lens's aberration. The only fundamental aberration constraint imposed on the projection lens is that a reverse ray trace of a full-aperture ray bundle from any design focal point on the image plane to the object surface should have a geometric point spread on the object surface that is small in relation to the spot separation.

In a variation of the Fig. 5 configuration, the aberration-correction function would not be performed by the microlenses, but would be performed by separate phase-modifying surfaces that correct for aberrations in both the microlenses and the projection lens. The aberration-correcting surface shapes could be formed, e.g., by means of a scanned ion-etch process, to compensate for interferometrically measured wavefront aberrations of the as-built optical system.

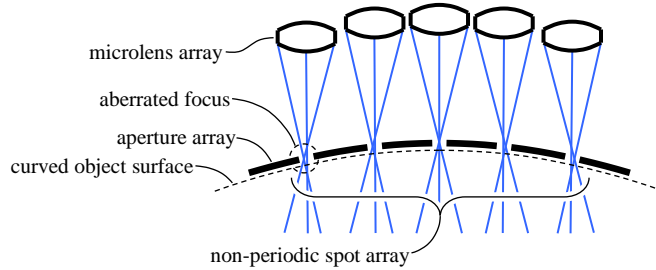


Fig. 5 Spot-generation optics adapted to projection lens

3. Narrow-band achromatization

An optical system can be achromatized by means of a “phase-Fresnel” lens surface, which is a type of Fresnel lens that is designed to preserve optical phase coherence between lens facets [6-9]. The achromatization procedure is illustrated in Fig's. 6(a) and 6(b), which depict cross-sectional views of a conventional, refracting lens surface (Fig. 6(a)) and a faceted, phase-Fresnel surface (Fig. 6(b)). In either case, the surface separates an index- n optical medium on the object side from an index- n' medium on the image side. For any particular wavelength, a specific object point gives rise to an electromagnetic field having a position-dependent phase Φ on the surface's object side, and the conjugate image point similarly has an associated phase function Φ' on the image side. (The phase functions are each specified within an undetermined additive constant.) Geometric waves are constant-phase surfaces, and geometric rays are directed along the phase gradient.

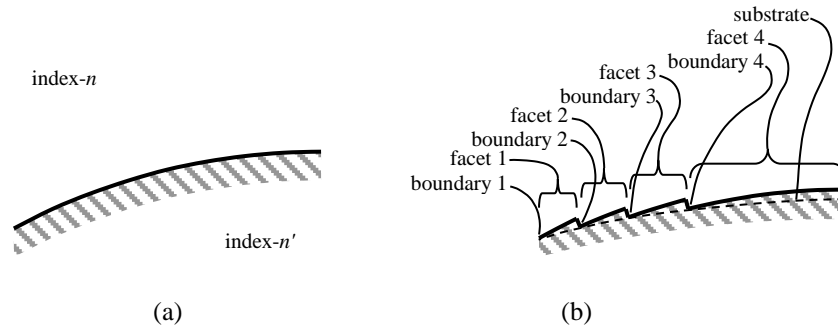


Fig. 6. A refracting lens surface (a) and a phase-Fresnel surface (b).

The simple refracting surface geometry (Fig. 6(a)) is defined by a phase-matching criterion,

$$\Phi' = \Phi + C \quad \text{on the lens surface} \quad (1)$$

where “ C ” is a constant term, which is determined by specifying the location of a particular point on the surface. (C is “constant” in the sense of being position-independent, but is a function of wavelength.) For a phase-Fresnel surface (Fig. 6(b)) that is blazed for maximum efficiency at a particular wavelength in the m -th diffraction order, an equation similar to Eq. (1) applies on the facet surfaces, except that the constant term jumps discontinuously by $m2\pi$ between facets,

$$\Phi' = \Phi + jm2\pi + C \quad \text{on facet } j \text{ (at } m\text{-th order blaze wavelength)} \quad (2)$$

In this equation j is a sequential facet numbering index (1, 2, ... in Fig. 6(b)) and C is implicitly a function only of wavelength. (The plus sign preceding j in Eq. (2) could alternatively be minus, depending on the adopted sign conventions for facet and order indexing.)

For an arbitrary wavelength other than the blaze wavelength, Eq. (2) does not generally hold, but it does hold on the facet boundaries for the m -th diffraction order’s phase function Φ' ,

$$\Phi' = \Phi + jm2\pi + C \quad \text{on boundary } j \text{ (in } m\text{-th order, any wavelength)} \quad (3)$$

The grating preserves phase coherence between corresponding points (e.g., boundary points) on different facets, although diffraction efficiency will generally be degraded due to dephasing between points on the same facet unless Eq. (2) holds. According to Eq. (3) the phase distribution Φ' in any particular diffraction order does not depend on the detailed surface geometry; it only depends on the geometry of the facet boundaries. The facet surface shape only determines the energy partitioning between diffraction orders.

A phase-Fresnel surface cannot be blazed for multiple wavelengths in a particular diffraction order, but Eq. (3) can be imposed for arbitrary phase functions Φ and Φ' at two distinct wavelengths,

$$\Phi'_1 = \Phi_1 + jm2\pi + C_1, \quad \Phi'_2 = \Phi_2 + jm2\pi + C_2 \quad \text{on boundary } j \quad (4)$$

In this equation Φ_1 and Φ'_1 are phase functions associated with a particular wavelength λ_1 ; Φ_2 and Φ'_2 are phase functions associated with a second wavelength λ_2 ; and C_1 and C_2 are constants. The two equalities in Eq’s. (4) define two surfaces whose intersection is a three-dimensional curve defining boundary j . The difference between the two equalities defines the grating “substrate,” an imaginary smooth surface that includes the boundaries (Fig. 6(b)),

$$\Phi'_1 - \Phi'_2 = \Phi_1 - \Phi_2 + C_1 - C_2 \quad \text{on substrate} \quad (5)$$

The above design procedure achieves two-wavelength achromatization in diffraction order m at wavelengths λ_1 and λ_2 . Narrow-band achromatization can be achieved by taking λ_1 and λ_2 to be infinitesimally close to the blaze wavelength, in which case Eq. (5) translates to a differential relation of the form

$$\frac{\partial \Phi'}{\partial \lambda} = \frac{\partial \Phi}{\partial \lambda} + \frac{dC}{d\lambda} \quad \text{on substrate (at blaze wavelength)} \quad (6)$$

The conjunction of Eq's. (3) and (6) defines the boundary of facet j . The $dC/d\lambda$ term in Eq. (6) is defined (at the blaze wavelength) by specifying the location of any particular point on the substrate, and the C term in Eq. (3) is defined by specifying any particular facet boundary point.

For the refracting surface of Fig. 6(a), the phase continuity condition (Eq. (1)) implies continuity of the surface-tangential phase gradient. The magnitude of the phase gradient in an index- n medium is $2\pi n/\lambda$ based on the eikonal equation [10], so the phase continuity condition translates to Snell's Law (see Fig. 7(a)),

$$n' \sin \theta' = n \sin \theta \quad (7)$$

For a grating surface, a similar equation is obtained from Eq. (3). The equation only applies on the facet boundaries, but can be smoothly interpolated between boundaries to define a continuous relationship over the entire substrate surface. (In the interpolated relationship, the j index becomes a smooth function of position, which takes on integer values on the facet boundaries.) The surface-tangential gradient of the interpolated relationship on the substrate translates to the grating equation for order m ,

$$n' \sin \theta' = n \sin \theta + m \lambda / d \quad (8)$$

where d is the grating period and the angles θ and θ' are defined relative to the substrate surface (Fig. 7(b)). (This form of the grating equation applies to meridional rays in an axisymmetric optical system; it is not generally applicable to skew rays and decentered or asymmetric systems.) At the blaze wavelength, Eq. (2) applies over each facet surface and Snell's Law applies with the angles defined relative to the facet surface,

$$n' \sin[\theta' - \alpha] = n \sin[\theta - \alpha] \quad (\text{at blaze wavelength}) \quad (9)$$

This "blaze condition" determines the facet angle,

$$\alpha = \tan^{-1} \left[\frac{n' \sin \theta' - n \sin \theta}{n' \cos \theta' - n \cos \theta} \right] \quad (\text{at blaze wavelength}) \quad (10)$$

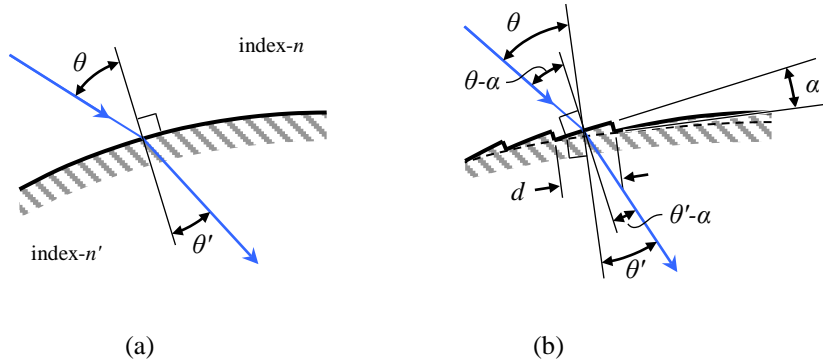


Fig. 7. Ray geometry for (a) Eq. (7), and (b) Eq's. (8) and (9).

Figure 8(a) shows an illustrative example of a phase-Fresnel grating that is configured to achieve narrow-band achromatization of a prism at a blaze wavelength of $0.266 \mu\text{m}$. Both elements are fused silica (SiO_2), which has a dispersion characteristic defined by a Sellmeier equation [11]. (The refractive index is 1.5 at $0.266 \mu\text{m}$.) As illustrated schematically in Fig. 8(a), the prism is configured to deflect a collimated beam at the $0.266\text{-}\mu\text{m}$ wavelength

symmetrically by 45° . The achromatizer has zero power (i.e., the $0.266\text{-}\mu\text{m}$ wavelength is not deviated by the achromatizer, which functions only to neutralize the prism's chromatic dispersion).

Figure 8(b) shows detail of a Fresnel facet, which has a sawtooth structure with a $1.53\text{-}\mu\text{m}$ period and 20.4° facet angle. The figure also shows a modified facet form (gray curve), which has rounded profile corners to improve manufacturability, and which is also configured to suppress the zero and second diffraction orders. The corners have a quarter-wave ($0.0665\text{-}\mu\text{m}$) radius and are connected by tangential Cornu spline segments [12]. Profile coordinate data for the two profile forms illustrated in Fig. 8(b) are tabulated in the Appendix.

Figure 9 illustrates the prism's first-order dispersion characteristic (θ'_2 versus λ) with and without achromatization. With achromatization, the slope $d\theta'_2/d\lambda$ is zero at the $0.266\text{-}\mu\text{m}$ blaze wavelength.

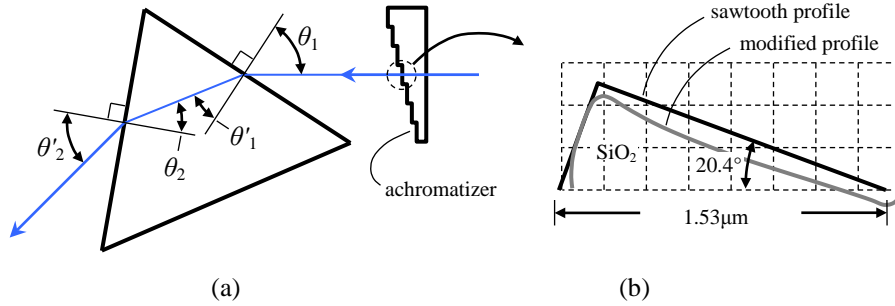


Fig. 8. (a) Phase-Fresnel achromatizer for prism designed to symmetrically deflect a $0.266\text{-}\mu\text{m}$ wavelength by 45° (i.e., $\theta_1 - \theta'_1 = \theta'_2 - \theta_2 = 22.5^\circ$); (b) detail of grating facet geometry (one period) on a $0.2\text{-}\mu\text{m}$ grid.

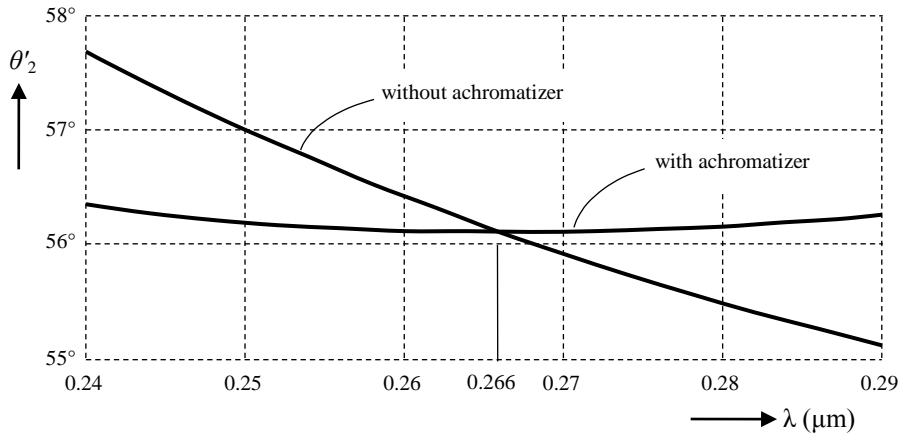


Fig. 9. Prism dispersion with and without achromatizer.

Table 1 shows the multi-order transmitted diffraction efficiencies of both the sawtooth and modified grating structures illustrated in Fig. 8(b), for both TE and TM polarization, at the $0.266\text{-}\mu\text{m}$ blaze wavelength. (The calculated efficiencies are based on a Kirchhoff boundary-integral method similar to [13]. “TE” corresponds to the E-field polarization being parallel to the grating lines.) There is some energy loss to reflection, which is not accounted for in Table

1. The “Scatter” is the sum of transmission efficiencies, excluding the first order. The scatter could be problematic in a lithography application, in which it would contribute to image haze, but in a confocal microscopy application the scatter would be blocked by the confocal aperture-filtering mechanism in the optical path from the inspection surface to the detector. Also, if phase-Fresnel surfaces are used in the spot generation optics, then the spot-delimiting apertures (Fig. 5) would block much of the forward scatter. Only the diffraction orders proximate the first order (e.g. the zero and second orders) would potentially be problematic.

The light scatter into extraneous diffraction orders could be greatly reduced by forming the grating on a high-refractive-index medium. Also, phase-Fresnel gratings can be formed as reflections gratings, which would exhibit much less scatter.

Table 1. Transmission Diffraction Efficiencies of Fig. 8(b) Grating

Order	Efficiency			
	TE		TM	
	Sawtooth	Modified	Sawtooth	Modified
-3	3.13%	2.92%	4.07%	4.24%
-2	2.23%	2.28%	2.55%	2.81%
-1	1.74%	1.46%	1.81%	1.59%
0	1.39%	0.47%	1.30%	0.70%
1	80.74%	83.58%	79.96%	83.37%
2	1.43%	0.59%	1.16%	0.59%
3	0.98%	1.81%	0.71%	1.09%
4	0.48%	1.25%	0.33%	0.53%
5	0.093%	0.33%	0.063%	0.071%
6	0.052%	0.042%	0.00064%	0.0056%
7	0.052%	0.048%	0.0075%	0.020%
Scatter	11.57%	11.20%	11.99%	11.64%

A phase-Fresnel grating could be formed on a projection lens surface by depositing a machinable, sacrificial layer on the surface, diamond-point turning the Fresnel surface pattern in the layer, and then transferring the pattern to the glass substrate by applying a blanket plasma etch. (The etch process would mitigate high-spatial-frequency roughness resulting from the machining process.) Alternatively, the pattern could be formed by a grey-scale lithographic process, using a laser-writing exposure tool similar to a machining lathe in which the cutting tool is replaced by a focused exposure beam. Phase-Fresnel structures could be formed in the spot-generation micro-optics by using more conventional microfabrication techniques.

A phase-Fresnel projection lens surface can achieve two-wavelength or narrow-band correction of axial color, but because the above-described design procedure can only be applied for a particular image point a single phase-Fresnel surface could not be configured to also correct lateral color. However, this would not be a limitation if achromatizing phase-Fresnel surfaces are formed in the spot-generation optics (e.g., on the microlens surfaces in Fig. 5), because each such surface would only transmit radiation to a single geometric image point. Thus, the spot-generation optics could be configured to achieve full-field achromatization.

A practical design approach may be to use a phase-Fresnel projection lens surface to perform most of the achromatization, and to use phase-Fresnel spot-generation elements only to eliminate any residual chromatic aberration. This would minimize the number of facets that must be formed on the micro-optics elements.

4. Polarization control

In high-NA lithography systems it is desirable to control the exposure radiation’s polarization state so that the radiation is horizontally polarized at the (horizontal) image plane. This

condition optimizes print resolution, and it also has the advantage that the projection lens can use a uniaxial birefringent glass, such as sapphire, for the last lens element [14].

Sub-wavelength grating structures exhibit form birefringence [15], which can be used for polarization control in lithography projection lenses. A form-birefringent quarter-wave plate comprising a lamellar grating structure is illustrated in cross-section in Fig. 10. Figure 11 shows a plan view of such an element, comprising curved grating lines, which could be positioned in a projection lens's aperture plane to convert circularly-polarized incident radiation into azimuthally-polarized transmitted radiation [16]. (The structure described in [16] is designed for infrared operation, but the same principle would apply to DUV lithography.) The grating lines form a 45° angle with any radial vector through the lens axis, and the arrows in Fig. 11 illustrate the transmitted polarization direction. (The central portion of the grating element is masked.)

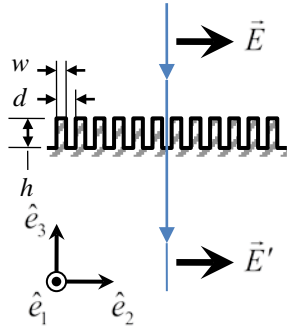


Fig. 10. Form-birefringent quarter-wave plate.

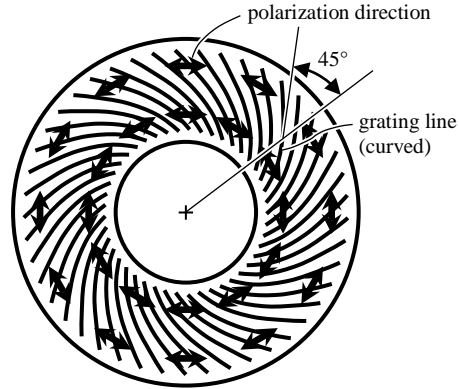


Fig. 11. Form-birefringent polarization control element.

Table 2 provides illustrative design parameters for a quarter-wave phase plate having the form of Fig. 10, comprising lamellar nitride (Si_3N_4) lines on a fused-silica (SiO_2) substrate. The grating is designed for 0.266- μm radiation. (The SiO_2 refractive index is 1.5 at 0.266 μm .) Each row of the table represents a design in which the period (d) is specified and the grating line width (w) and height (h) are determined to satisfy two conditions: The grating should induce a phase difference of $\pi/2$ between TE and TM polarization, and within this constraint the grating height is minimized. (The table data were calculated using a commercial coupled-wave grating analysis program, GD-Calc® [17].)

Table 2. Design parameters for a $\text{Si}_3\text{N}_4/\text{SiO}_2$ form-birefringent quarter-wave plate operating at 0.266 μm

d (μm)	w/d	h (μm)	d (μm)	w/d	h (μm)
0.05000	0.5595	0.15819	0.11000	0.4021	0.15776
0.06000	0.5345	0.15938	0.12000	0.3775	0.15551
0.07000	0.5077	0.16018	0.13000	0.3535	0.15236
0.08000	0.4806	0.16048	0.14000	0.3307	0.14784
0.09000	0.4536	0.16020	0.15000	0.3109	0.14075
0.10000	0.4274	0.15930			

A fundamental limitation of the Fig. 11 device is that it cannot be configured to produce the desired polarization state for rays traversing the device from all object field points. It can be optimized for the center of the field, and it may exhibit generally good performance for

meridional rays, but the design does not have sufficient degrees of freedom to optimally control the polarization state of all rays including skew rays. This limitation can be overcome by incorporating form-birefringent surfaces in the spot-generation optics (Fig. 5), as a sub-wavelength pattern on the microlenses or on separate optical surfaces in series with the microlenses. Since each point on such a surface is traversed by only one design geometric ray, the local surface structure at that point need only be optimized for a single ray, and the polarization-control system can thus be optimized for all rays.

A practical design approach may be to use an aperture-plane phase plate, such as that illustrated in Fig. 11, to perform most of the polarization control, and to use the spot-generation optics only to correct residual polarization errors. If the residual errors are small, comparatively shallow form-birefringent elements could be used to make the corrections, and the correction element designs could be optimized based on polarimetric metrology data for the as-built projection lens.

The form-birefringent elements would typically comprise curved grating elements with a nonuniform period, width and depth, which may be formed on a curved substrate. The design principle of the polarization-control optics can be illustrated by considering, for simplicity, normal incidence on a uniform sub-wavelength grating. The grating substrate is parallel to coordinate basis vectors \hat{e}_1 and \hat{e}_2 (Fig. 10). The incident E-field's polarization vector \vec{E} and the transmitted E-field's polarization vector \vec{E}' have coordinate projections of the form

$$\vec{E} = E_1 \hat{e}_1 + E_2 \hat{e}_2, \quad \vec{E}' = E'_1 \hat{e}_1 + E'_2 \hat{e}_2 \quad (11)$$

(The vector components are generally complex-valued.) \vec{E} would be defined by calculating a polarization ray trace from the radiation source to the grating, and \vec{E}' would be defined by performing a reverse polarization ray trace from the image plane, where the E-field is horizontally polarized, to the grating.

The incident and transmitted field amplitudes are related by a Jones matrix transformation of the form

$$\begin{pmatrix} E'_1 \\ E'_2 \end{pmatrix} = \begin{pmatrix} \cos[\theta] & -\sin[\theta] \\ \sin[\theta] & \cos[\theta] \end{pmatrix} \begin{pmatrix} t_1 & 0 \\ 0 & t_2 \end{pmatrix} \begin{pmatrix} \cos[\theta] & \sin[\theta] \\ -\sin[\theta] & \cos[\theta] \end{pmatrix} \begin{pmatrix} E_1 \\ E_2 \end{pmatrix} \quad (12)$$

where t_1 and t_2 are grating's complex transmittance factors for TE and TM, respectively, and θ is the grating lines' rotation angle from the \hat{e}_1 direction toward \hat{e}_2 . (Note: This paper follows the Mathematica convention of using square braces [...] as function argument delimiters and round braces (...) for grouping.) For an ideal form-birefringent phase plate t_1 and t_2 would have the same magnitude and would differ only in phase, but in practice they may differ in magnitude even if the device has no optical absorption, because the phase plate may exhibit polarization-dependent reflection losses.

The incident and transmitted beams' polarization states are defined by the complex ratios E_1 / E_2 and E'_1 / E'_2 , respectively, and satisfy the following relationship based on Eq. (12),

$$1 + \rho = (1 - \rho) \left(\cos[2\theta] \frac{P + P'}{P - P'} + \sin[2\theta] \frac{1 - P P'}{P - P'} \right) \quad (13)$$

where

$$\rho = t_1 / t_2 \quad (14)$$

$$P = E_1 / E_2 \quad (15)$$

$$P' = E'_1 / E'_2 \quad (16)$$

The real and imaginary parts of Eq. (13) define two design conditions that should be satisfied by the selection of ρ and θ . Since ρ is complex-valued, the grating design has an extra degree of freedom that can be used to satisfy another design condition (e.g., minimizing the grating height).

For a quarter-wave plate that is configured to convert circularly-polarized incident radiation into transmitted radiation that is linearly polarized parallel to \hat{e}_2 , the above equations take the following form,

$$\vec{E} = \hat{e}_1 + i\hat{e}_2, \quad \vec{E}' = \hat{e}_2 \rightarrow P = -i, \quad P' = 0, \quad \rho = i \tan[\theta] \quad (17)$$

If the grating is configured to balance the transmittance intensity between TE and TM polarizations (i.e., $|\rho|=1$), then Eq. (17) implies that $\theta = 45^\circ$ (as illustrated in Fig. 11). However, there is no need to impose this condition because any intensity mismatch between TE and TM can be accommodated by setting $\tan[\theta]=|\rho|$ according to Eq. (17). In any case, Eq. (17) implies that the grating should induce a 90° phase shift between the TE and TM polarization modes (because ρ is a real multiple of i).

5. Beam intensity control

A geometric ray's E-field vector \vec{E}' can be described in terms of two complex-valued scalar components E'_1 and E'_2 , as in Eq. (11), after the ray has passed through the spot-generation optics of Fig. 5 including any associated aberration-control, achromatizing, and polarization-control elements. E'_1 and E'_2 can be represented in terms of their magnitude and phase,

$$E'_1 = |E'_1| \exp[i\phi'_1], \quad E'_2 = |E'_2| \exp[i\phi'_2] \quad (18)$$

\vec{E}' can be further defined in terms of four scalar quantities, $\frac{1}{2}(\phi'_1 + \phi'_2)$, $(\phi'_1 - \phi'_2)$, $|E'_1 / E'_2|$ and $|E'_1|^2 + |E'_2|^2$:

$$E'_1 = \sqrt{\frac{|E'_1|^2 + |E'_2|^2}{1 + |E'_2 / E'_1|^2}} \exp[i(\frac{1}{2}(\phi'_1 + \phi'_2) + \frac{1}{2}(\phi'_1 - \phi'_2))] \quad (19)$$

$$E'_2 = \sqrt{\frac{|E'_1|^2 + |E'_2|^2}{1 + |E'_1 / E'_2|^2}} \exp[i(\frac{1}{2}(\phi'_1 + \phi'_2) - \frac{1}{2}(\phi'_1 - \phi'_2))] \quad (20)$$

The first of the quantities, $\frac{1}{2}(\phi'_1 + \phi'_2)$, represents the average phase of E'_1 and E'_2 , which is determined by the aberration-control element. The second and third quantities, $(\phi'_1 - \phi'_2)$ and $|E'_1 / E'_2|$, are determined by P' (Eq. (16)), which can be determined by a form-birefringent polarization-control element. The last term, $|E'_1|^2 + |E'_2|^2$, which represents the radiant intensity in the transmitted ray, can be determined by a beam intensity-control element. (Intensity control would be useful, for example, for maintaining exposure dose uniformity in a lithography system.) With all of these elements in place, each transmitted ray's vector complex amplitude \vec{E}' could be fully and individually controlled to a design specification.

An optically absorbing film could be formed on, or in series with, each microlens in the spot-generation optics (Fig. 5) to control beam intensity. A graded-thickness absorbing film would provide full control over each spot beam's intensity profile. Alternatively, a non-absorbing diffraction grating could be used to attenuate the transmitted zero-order intensity by shunting energy into first and higher diffraction orders. (The aperture array in Fig. 5 would block the diffracted energy.)

If a polarization-neutral attenuator is needed, then a biperiodic grating such as a square array of circular posts could be used, as illustrated in Fig. 12(a). However, there would be no need to require polarization neutrality if the optics include polarization control, as described in Section 4. Polarization and intensity control could be provided by a single optical surface such as that illustrated in Fig. 12(b). The surface comprises a superposition of two crossed grating patterns, a sub-wavelength grating that exhibits form birefringence for polarization control, and a coarse grating pattern that diffractively attenuates the zero order. The gratings' structural parameters (e.g., line orientation, line width, depth) could vary nonuniformly across the grating aperture to provide full control over the E-field's spatial distribution.

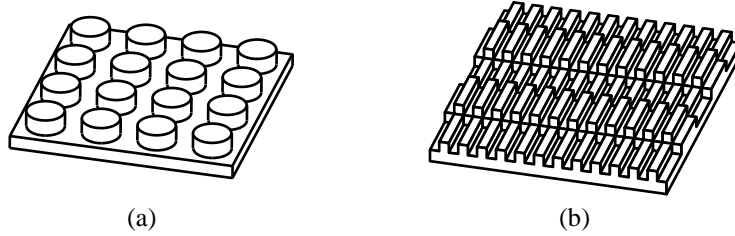


Fig. 12. A diffractive attenuator formed (a) as a square array of circular posts, or (b) as a crossed grating including a form-birefringent polarization-control structure.

6. Multi-function spot-generation optics

The spot-generation optics can include any or all of the above-described mechanisms in a multi-function device, as illustrated schematically in Fig. 13. In this illustration the elements that generate a particular object spot are represented as separate, sequential optical surfaces, but some or all of the surfaces could be combined into a single surface pattern comprising multiple structures at different dimensional scales for performing multiple optical functions.

The elements in Fig. 13 include: (1) a surface-contoured phase plate, which operates as a geometric aberration corrector, (2) a stepped, phase-Fresnel surface, which provides narrow-band achromatization, (3) a sub-wavelength, form-birefringent polarization control element, (4) a diffractive zero-order attenuator for controlling the spot beam's intensity profile, (5) a microlens, which focuses illumination onto an object spot conjugate to a design image point, and (6) a spot-delimiting aperture, which blocks stray light.

These elements can operate in combination to provide full control over each spot beam's E-field distribution in the projection lens's object space, thereby relieving the projection lens design requirements. Moreover, the micro-optics fabrication process can be optimized to utilize interferometric and polarimetric metrology data on the as-built projection lens, thereby relieving lens manufacturing tolerances. Such capabilities have the potential of overcoming fundamental limitations of conventional optical systems and shifting the technology base of the microlithography and inspection microscopy industries from massive, monolithic optics to precision-engineered micro-optics.

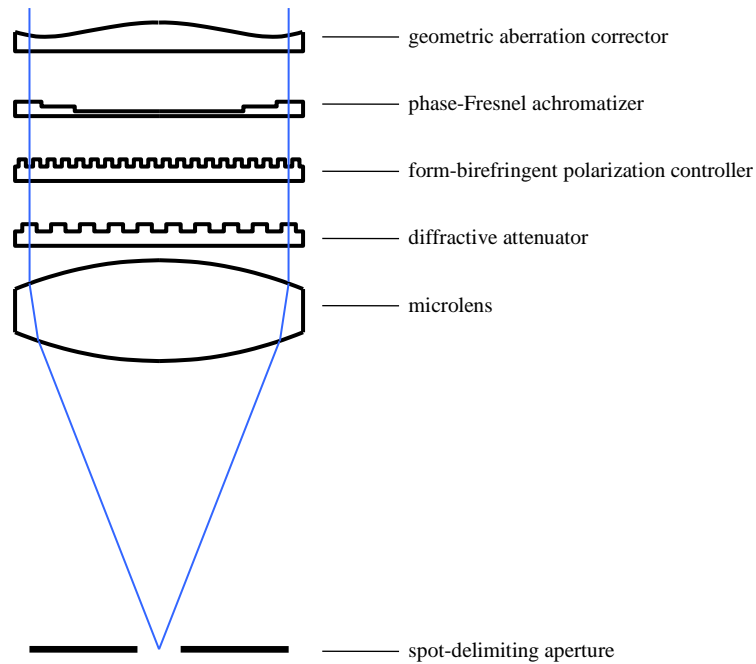


Fig. 13. Multi-function spot-generation optics.

Appendix: Profile coordinate data for phase-Fresnel gratings of Fig. 8(b)

Following are coordinate data representing X (horizontal) and Y (vertical) profile coordinates for points on the two grating profiles illustrated in Fig. 8(b). These listings represent the partitioning of the profiles into integration intervals for the Kirchhoff-integral diffraction calculations used to generate the data in Table 1. All coordinates are in microns. The grating period is 1.5290 μm , and the last data point in each profile listing represents a one-period shift of the first point.

Sawtooth profile		Modified profile	
X	Y	X	Y
0	0	0.06573	0.01009
-0.0249	0.0092483	0.064513	-0.016136
-0.049801	0.018497	0.053241	-0.039846
-0.074701	0.027745	0.03367	-0.057346
-0.099602	0.036993	0.0088525	-0.065908
-0.1245	0.046241	-0.017345	-0.064198
-0.1494	0.05549	-0.042266	-0.055421
-0.1743	0.064738	-0.067161	-0.046555
-0.1992	0.073986	-0.092105	-0.037826
-0.2241	0.083235	-0.11709	-0.029226
-0.249	0.092483	-0.14212	-0.020742
-0.27391	0.10173	-0.16719	-0.012366
-0.29881	0.11098	-0.19228	-0.0040861
-0.32371	0.12023	-0.21741	0.004107
-0.34861	0.12948	-0.24256	0.012224
-0.37351	0.13872	-0.26773	0.020276
-0.39841	0.14797	-0.29292	0.028272
-0.42331	0.15722	-0.31812	0.036224
-0.44821	0.16647	-0.34333	0.044141
-0.47311	0.17572	-0.36855	0.052035

-0.49801	0.18497	-0.39378	0.059915
-0.52291	0.19421	-0.419	0.067793
-0.54781	0.20346	-0.44422	0.075678
-0.57271	0.21271	-0.46944	0.083582
-0.59761	0.22196	-0.49465	0.091515
-0.62251	0.23121	-0.51985	0.099487
-0.64741	0.24046	-0.54503	0.10751
-0.67231	0.2497	-0.57019	0.11559
-0.69721	0.25895	-0.59532	0.12374
-0.72211	0.2682	-0.62044	0.13198
-0.74701	0.27745	-0.64552	0.1403
-0.77192	0.2867	-0.67056	0.14873
-0.79682	0.29595	-0.69557	0.15727
-0.82172	0.30519	-0.72054	0.16593
-0.84662	0.31444	-0.74546	0.17472
-0.87152	0.32369	-0.77033	0.18366
-0.89642	0.33294	-0.79515	0.19275
-0.92132	0.34219	-0.8199	0.202
-0.94622	0.35144	-0.84459	0.21142
-0.97112	0.36068	-0.86921	0.22103
-0.99602	0.36993	-0.89375	0.23083
-1.0209	0.37918	-0.91821	0.24083
-1.0458	0.38843	-0.94259	0.25104
-1.0707	0.39768	-0.96687	0.26147
-1.0956	0.40692	-0.99105	0.27213
-1.1205	0.41617	-1.0151	0.28303
-1.1454	0.42542	-1.0391	0.29418
-1.1703	0.43467	-1.0629	0.30559
-1.1952	0.44392	-1.0866	0.31726
-1.2201	0.45317	-1.1102	0.3292
-1.245	0.46241	-1.1336	0.34142
-1.2699	0.47166	-1.1569	0.35394
-1.2948	0.48091	-1.18	0.36675
-1.3197	0.49016	-1.203	0.37986
-1.344	0.49801	-1.2257	0.39329
-1.3532	0.47311	-1.2483	0.40704
-1.3625	0.44821	-1.2707	0.42111
-1.3717	0.42331	-1.2938	0.4337
-1.381	0.39841	-1.3198	0.43715
-1.3902	0.37351	-1.3452	0.43026
-1.3995	0.34861	-1.3659	0.4141
-1.4087	0.32371	-1.3792	0.3914
-1.418	0.29881	-1.3903	0.36741
-1.4272	0.27391	-1.401	0.34326
-1.4365	0.249	-1.4113	0.31893
-1.4457	0.2241	-1.4211	0.29438
-1.455	0.1992	-1.4302	0.26959
-1.4642	0.1743	-1.4386	0.24454
-1.4735	0.1494	-1.4462	0.21922
-1.4827	0.1245	-1.4528	0.19364
-1.492	0.099602	-1.4584	0.1678
-1.5012	0.074701	-1.4628	0.14174
-1.5105	0.049801	-1.4659	0.1155
-1.5197	0.0249	-1.4676	0.089133
-1.529	0	-1.4678	0.062711
		-1.4663	0.036326
		-1.4632	0.01009